Strength and stability of point-symmetric cold-formed steel members undergoing lateral-torsional buckling

Shuo Wang[1], Robert S. Glauz[2], Benjamin W. Schafer[3]

Abstract
The objective of this paper is to report on a series of numerical analyses performed to study the lateral-torsional buckling behavior of point-symmetric, typically Zee-shaped, cold-formed steel members. Zees have principal axes which are inclined from the geometric axes as defined by the web and flange. Further, loading and bracing is often in the geometric axes. As a result, stability and strength, even in the global lateral-torsional buckling mode is an unconventional coupling of torsion as well as major- and minor-principal axis bending. The governing design specification for these cold-formed steel members in North America, AISI S100, has long applied a conservative simplification for elastic lateral-torsional buckling of point-symmetric sections. Recently, the AISI subcommittee on Member Design, which the second author chairs, considered proposed changes for lateral-torsional buckling of point-symmetric and non-symmetric sections, but limited data was available to support these changes. The purpose of this study was to provide additional exploration of the proposed design approach using numerical analysis. Geometric and material nonlinear shell finite element analysis was conducted on Zees specifically selected to focus on global deformation, i.e., sections not prone to local or distortional buckling under the studied conditions. The results are compared with existing and proposed provisions for both stability and strength and recommendations provided for design.

1. Introduction
Cold-formed steel (CFS) members are formed by bending sheet steel into useful structural shapes. The resulting shapes are typically open in cross-section with limited torsional stiffness. In addition, such sections need not be symmetric, therefore flexural and torsional deformations are commonly coupled. However, the governing CFS design specification in North America, AISI S100, has long taken a simplistic approach to lateral-torsional buckling provisions for non-symmetric members.

---

[1] Graduate Research Assistant, Dept. of Civil and Systems Eng., Johns Hopkins University, <swang226@jhu.edu>
[2] President/Owner, RSG Software, Inc., <glauz@rsgsoftware.com>
[3] Professor, Dept. of Civil and Systems Eng., Johns Hopkins University, <schafer@jhu.edu>

Non-symmetric CFS members can potentially serve as efficient purlins, girts, joists, rack uprights, etc. Unlike conventional singly-symmetric cold-formed steel members, the support layout and the principal axes do not align for such members. For example, the common point-symmetric Zee-shaped sections that are the focus of the work herein, have principal axes inclined from the web and flange as shown in Figure 1. As a result of the location of the principal axis common gravity loading (for example in the -Y direction of Figure 1) causes bending about both principal axes – which leads to difficulty in determining the critical elastic lateral-torsional buckling stress. In addition to the geometric (X-Y) and principal (1-2) axes Figure 1b depicts another set of arbitrary axes (a-b) which are an angle θ from the principal major axis, and an angle β from the geometric axis. In the work herein, we will consider bending about the arbitrary axis "a" and the resulting global elastic buckling and strength.

Analytical formula for the elastic lateral-torsional (global) buckling for bending about any inclined axis ("a") from the major principal axis has recently been developed by Glauz (2017) and serves in part as motivation for this study. This paper considers the elastic bucking, inelastic buckling, and ultimate strength of typical Zee-shaped cold-formed steel members under the end moments of Figure 1. As discussed herein, members and details are selected to focus on global lateral-torsional buckling, not local or distortional buckling.
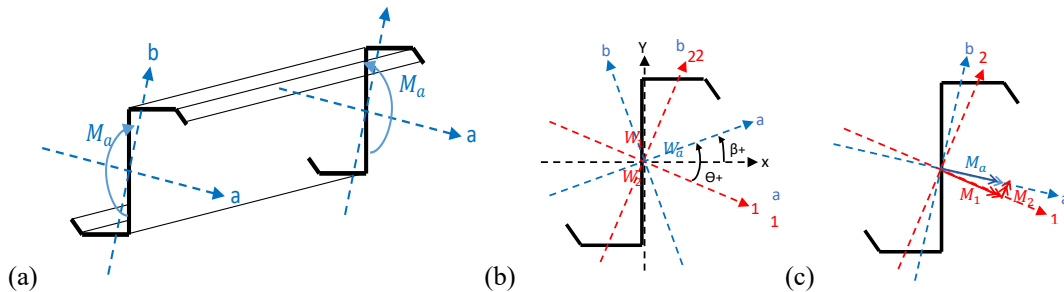

(a)   (b)   (c)

Figure 1: Zee section bent about non-principal axis (a) applied as end moments (b) coordinate axes and angles (c) decomposition of arbitrary axis bending moment into principal axis bending moments

2. Elastic Buckling about Arbitrary Bending Axis

Elastic lateral-torsional buckling (LTB) for bending about an axis not aligned with the major principal axis is an unusual case, not traditionally included in classical derivations or design specifications. This is true, in part, because the notion of "buckling" when the deformation resulting from the eigen problem is not orthogonal to the primary deformations from the loading, is a somewhat controversial concept. See Trahair (2018) for an explanation that rejects the possibility of buckling about the non-principal major axis. However, as Glauz (2017) shows analytically, and as is commonly implemented in finite strip and finite element software, the eigen problem whereby the magnitude of the linearized approximation of the geometric stiffness (K_g) erodes the elastic stiffness (K_e) is still well defined in these cases, i.e.:

$$K_e \phi = \lambda_{cr} K_g \phi \qquad (1)$$

Thus, a buckling load (λ_{cr} times the reference load) and mode (ϕ) may be established, even when the problem is not a pure bifurcation problem. For point-symmetric sections Glauz (2017) derives this moment to be:

$$M_{cre} = C_b r_o \sqrt{P_e P_t} \tag{2}$$

$$P_e = \frac{\pi^2 E I_1 I_2}{I_a (K_f L_f)^2} \tag{3}$$

$$P_t = \frac{1}{r_o^2}\left[GJ + \frac{\pi^2 E C_w}{(K_t L_t)^2}\right] \tag{4}$$

Where C_b is the moment gradient factor, r_o is the polar radius of gyration about the shear center, E is the modulus of elasticity, I_1 and I_2 are the principal moments of inertia, I_a is the moment of inertia about the axis of bending, $K_f L_f$ is the flexural effective length, G is the shear modulus, J is the St. Venant torsional stiffness, C_w is the warping stiffness, and $K_t L_t$ is the torsional effective length. For the studied Zee sections in Glauz (2017) bent about the geometric axis, i.e., perpendicular to the web, Eq. (2) is compared with plate finite strip solutions from CUFSM and CFS and shell finite element solutions from ABAQUS in Table 1. Cross-section properties for use in Eq.'s (2)-(4) are derived from sharp corner models in either CUFSM or CFS and are fully detailed in Wang et al. (2020). The methods are all in close agreement. This verifies that the elastic LTB calculation for bending about a non-principal axis is robust and can be performed by any of the selected methods with confidence.

Table 1: Buckling moment under unrestrained bending about geometric axis (X of Fig. 1)
for sharp corner Zee sections with F_y = 50 ksi and L = 180 in.

ID[1]	Analytical M_{cre}		FSM_M_{cre}		ABAQUS M_{cre}
	CUFSM[2]	CFS[2]	CUFSM	CFS	
	kip-in	kip-in	kip-in	kip-in	kip-in
12ZS3.25×105	158.891	158.407	157.627	157.330	157.320
12ZS2.75×105	112.134	111.807	111.509	111.270	111.336
12ZS2.25×105	75.119	74.922	74.860	74.749	74.774
10ZS3.25×105	128.093	127.655	127.429	127.060	127.157
10ZS2.75×105	90.878	90.575	90.565	90.346	90.407
10ZS2.25×105	61.340	61.133	61.224	61.080	61.142
9ZS2.25×105	54.739	54.537	54.669	54.530	54.588
8ZS3.25×105	99.246	98.850	98.921	98.590	98.685
8ZS2.75×105	70.927	70.643	70.793	70.565	70.651
8ZS2.25×105	48.373	48.180	48.337	48.204	48.259
7ZS2.25×105	42.291	42.105	42.280	42.149	42.202
6ZS2.25×105	36.553	36.371	36.560	36.426	36.483
4ZS2.25×70	14.799	14.733	14.800	14.746	14.771
3.5ZS1.5×70	5.306	5.277	5.317	5.292	5.310

1. Cross-section identification is (web depth in in.) ZS (flange width in in.) x (thickness in 1/1000 in.), additional dimensions per AISI D100 (2017) design manual.
2. Analytical formula of Glauz (2017) with cross-section properties generated from sharp corner model created in CUFSM or CFS as noted.

3. Shell Finite Element Modeling
A series of geometric and material nonlinear shell finite element models are developed in ABAQUS to explore the behavior of Zees bent about non-principal axes. A typical model is

depicted in Figure 2a. The Zee cross-section is meshed with the quadratic S9R5 shell element employing 20 elements across the web and 8 elements across the flange and lip and an aspect ratio of 1.0 along the length in the flange and near 1.0 throughout the section. The boundary conditions for the beam are an idealization of simply supported with warping free ends, this is achieved by restraining displacement in the plane of the cross-section at the member ends, and restraining longitudinal displacement of the cross-section at the mid-length as depicted in Figure 2a. The material is modeled as elastic-perfectly plastic implemented with von Mises yield criteria and isotropic hardening.

The loading in the ABAQUS model is with end moments, consistent with Figure 1a; however the end moments are converted to stress and applied as edge tractions similar to CUFSM as shown in Figure 2b. For each cross-section studied a series of different angles, defined by θ of Figure 1b, for the axis of bending are considered. For example for the 6ZS2.25×105 the applied reference moments (ABAQUS outputs are a scaler multiple of these moments) are provided in Table 2 along with the decomposition into principal moments consistent with Figure 1c.

Table 2: Applied bending moment decomposition vary with inclined bending axes.

	θ (degree)	$M_a=M_{ref}$	M_1	M_2
		kip-in	kip-in	kip-in
transition angle	-8	55.646	55.105	7.744
	-4	55.646	55.511	3.882
principal-major	0	55.646	55.646	0.000
	4	55.646	55.511	-3.882
	8	55.646	55.105	-7.744
transition angle	12	55.646	54.430	-11.570
	16	55.646	53.491	-15.338
	20	55.646	52.291	-19.032
geometric	23.481	55.646	51.039	-22.173
principal-minor	90	55.646	0.000	-55.646

In the ABAQUS nonlinear collapse analysis, the Riks solver is employed for equilibrium convergence. Note, no initial imperfections are considered in the initial collapse analysis. For any moment about non-principal axes there is always first order deformation in both principal axes – thus for global LTB the role of imperfections is less important. Imperfection sensitivity is explored further in Section 4.2.

Typical results are provided for analysis of the 6ZS2.25×105 section with $F_y = 50$ ksi and L=144 in. and bending about the geometric axis ($\theta = 23.481°$). Figure 3 provides the displaced shape and state of von Mises surface stress at peak load and in collapse, and Figure 4 provides the moment-deformation response of the section at mid-span. At peak moment neither local or distortional deformations are present – indicating that the section successfully isolates lateral-torsional buckling and yielding. In collapse, spatial mechanisms form shown as yielded zones in the stress contours and falling moment capacity in the moment-deformation plots. As the figures indicate the section experiences primary deformations (Z-direction in the ABAQUS model) as well as lateral deformations (Y-direction in the ABAQUS model) and twist.
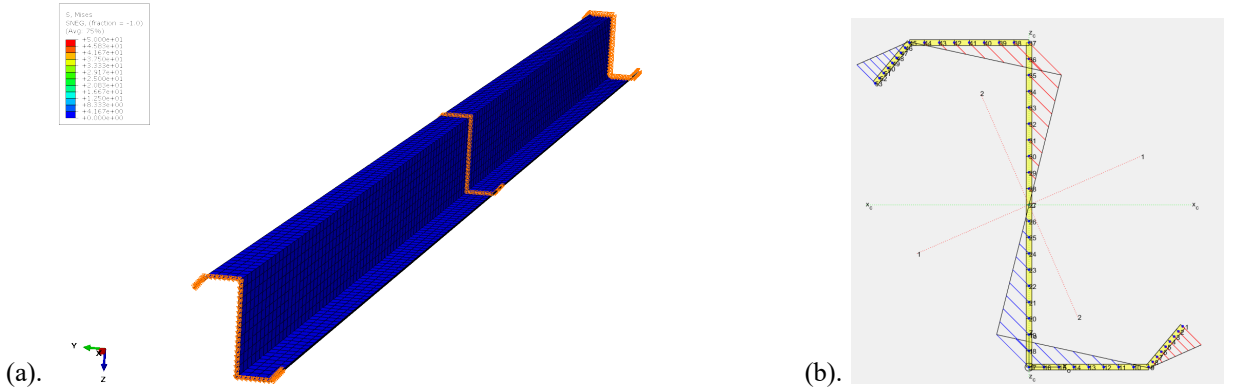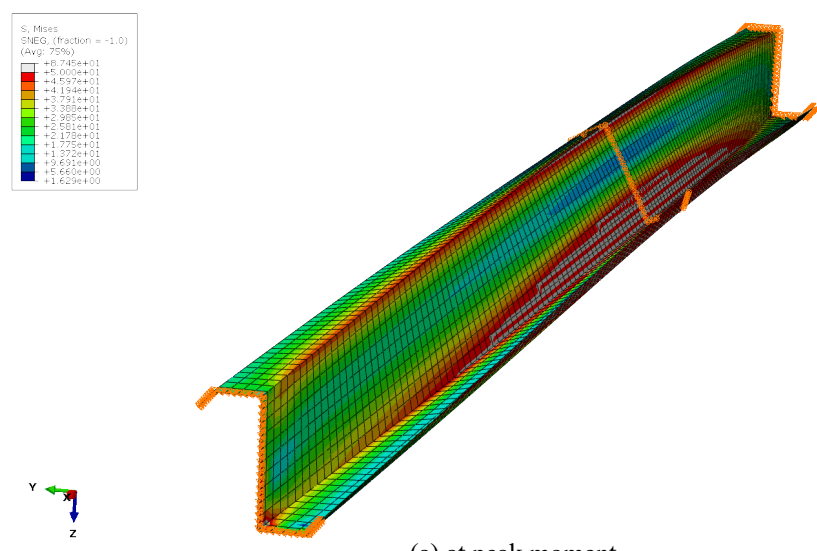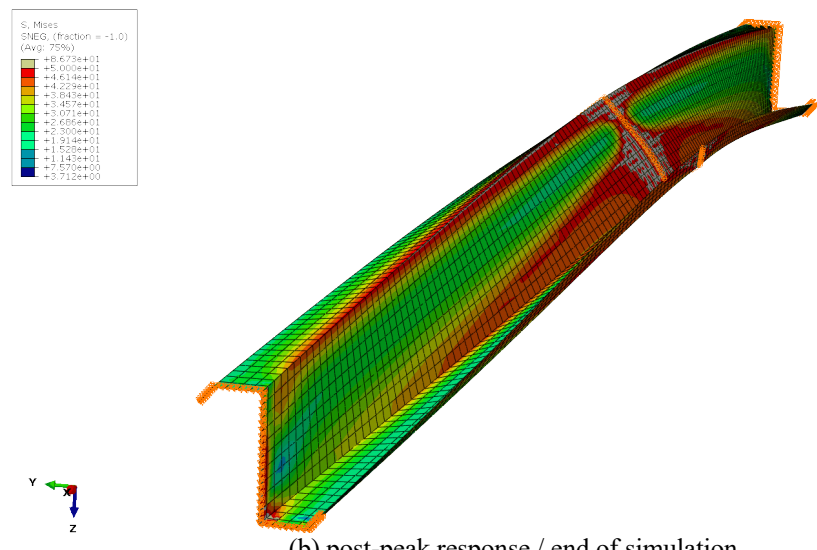
Figure 2: Finite element model (a) typical geometry (L=144 in.), boundary conditions, and mesh, (b) moment at end applied as stress, example shown for 6ZS2.25×105 section with θ=23.481° which is bending about geometric axis.
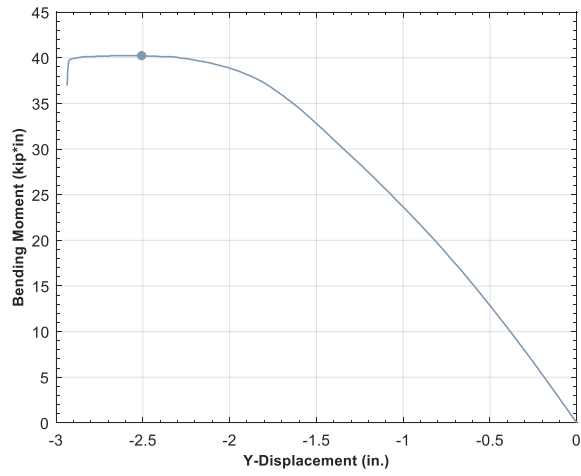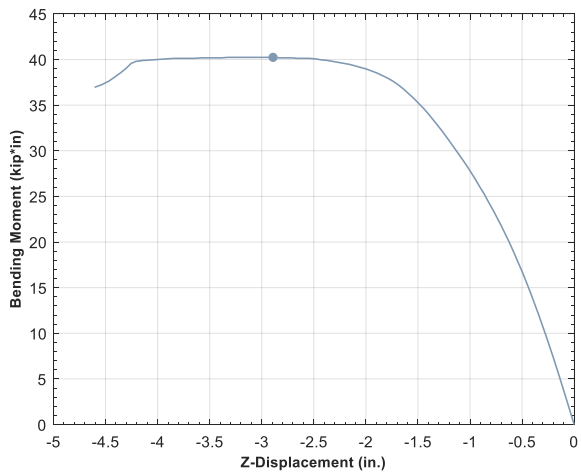

(a) at peak moment.

(b) post-peak response / end of simulation.
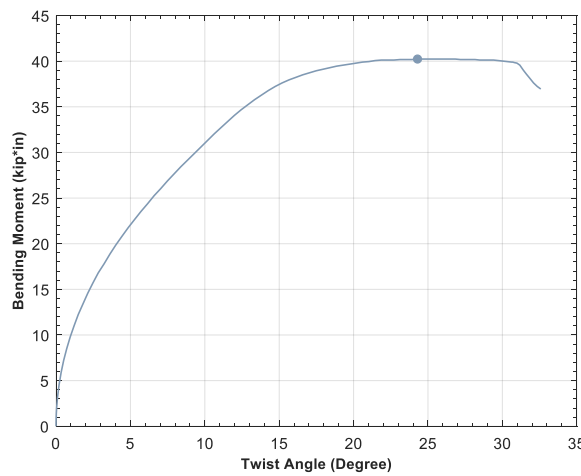
Figure 3: Shell surface von Mises stress displayed on magnified deformed shape for 6ZS2.25×105 section with θ=23.481°, i.e., bent about geometric axis, note grey = yielded (F_y = 50ksi).

(a).

(b).

(c).

Figure 4: Moment-deformation plots for 6ZS2.25×105 with F_y = 50 ksi and L = 144in at θ=23.481°. (a) lateral web deflection (x of Fig. 1, Y in ABAQUS model), (b) vertical web deflection (y in Fig. 1, Z in ABAQUS model), (c) web twist.

4. Parametric Study

To explore the response of the Zee sections across a variety of global slenderness values, the member length, L, and yield stress, F_y are varied as indicated in Table 3. To explore the impact of axis of bending, 10 angles for the axis of bending are considered: the two principal axes, the geometric axes, and 7 additional angles concentrated around the major principal axis. Two cross-sections, thick and stocky enough to avoid local and distortional buckling are selected: 6ZS2.25x105 and 10ZS2.25x105.

Table 3: Summary of parametric study cases.

| Section	Fy	L	θ
	(ksi)	(in.)	(degree)
6ZS2.25×105	33, 40, 50	144, 180, 240	-8, -4, 0, 4, 8, 12, 16, 20, 23.481, 90
10ZS2.25×105	33, 40, 50	144, 180, 240	-8, -4, 0, 4, 8, 11.711, 12, 16, 20, 90

Typical moment-deformation results for the 6ZS2.25×105 with F_y = 50 ksi and L = 144 in. are summarized in Figure 5, where (a) provides the moment vs. midspan lateral deformation, (b) the moment vs. midspan vertical deformation, and (c) the moment vs. midspan twist. Only the case with major principal axis bending, θ = 0°, exhibits classic bifurcation behavior in the large deflection solution. All analyses have a peak moment, +/- angles of inclination for the bending axis do not have symmetric response. Wang et al. (2020) provides plots and numerical results for all conducted analyses, however the results are generally typical to Figure 5.
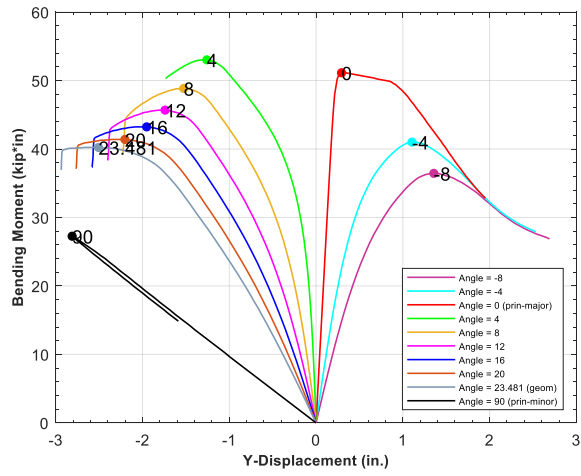
(a).
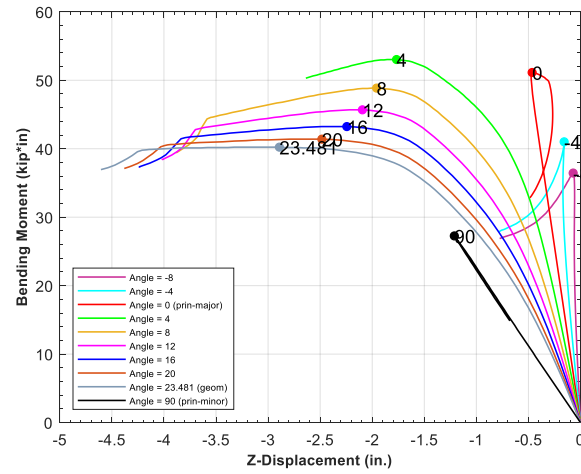
(b).
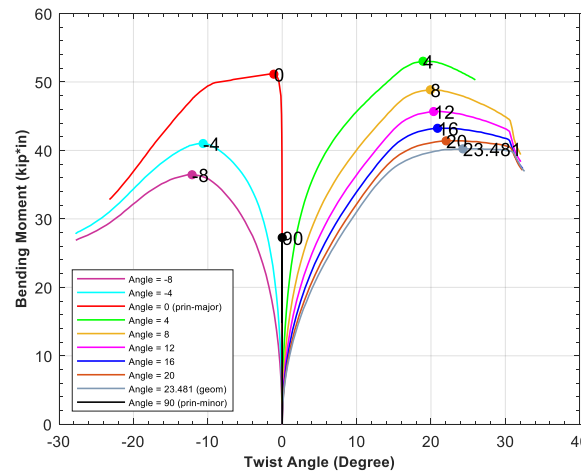
(c).

Figure 5: Moment-deformation plots for 6ZS2.25×105 with F_y = 50 ksi and L = 144 in. (a) lateral web deflection (x of Fig. 1, Y in ABAQUS model), (b) vertical web deflection (y in Fig. 1, Z in ABAQUS model), (c) web twist.

4.1 Failure mode sensitivity to inclination of bending axis

The lack of symmetry (i.e., compare moment-deformation at +8° vs. -8°) in the response for bending about the major principal axis, is at least initially surprising. However, when one considers the impact of the twist on the response the result can be understood more completely. As Figure 6 highlights for the 6ZS2.25×105, L=144 in., F_y=50 ksi – for bending about an axis inclined positively from the major principal axis peak, stresses occur at the flange/web juncture and the failure mechanism is a relatively benign spatial plastic mechanism in the web. However, for bending about an axis inclined negatively from the major principal axis, the peak stresses are at the flange/lip juncture, which leads to more pronounced instability and a less favorable flange/lip failure mechanism.
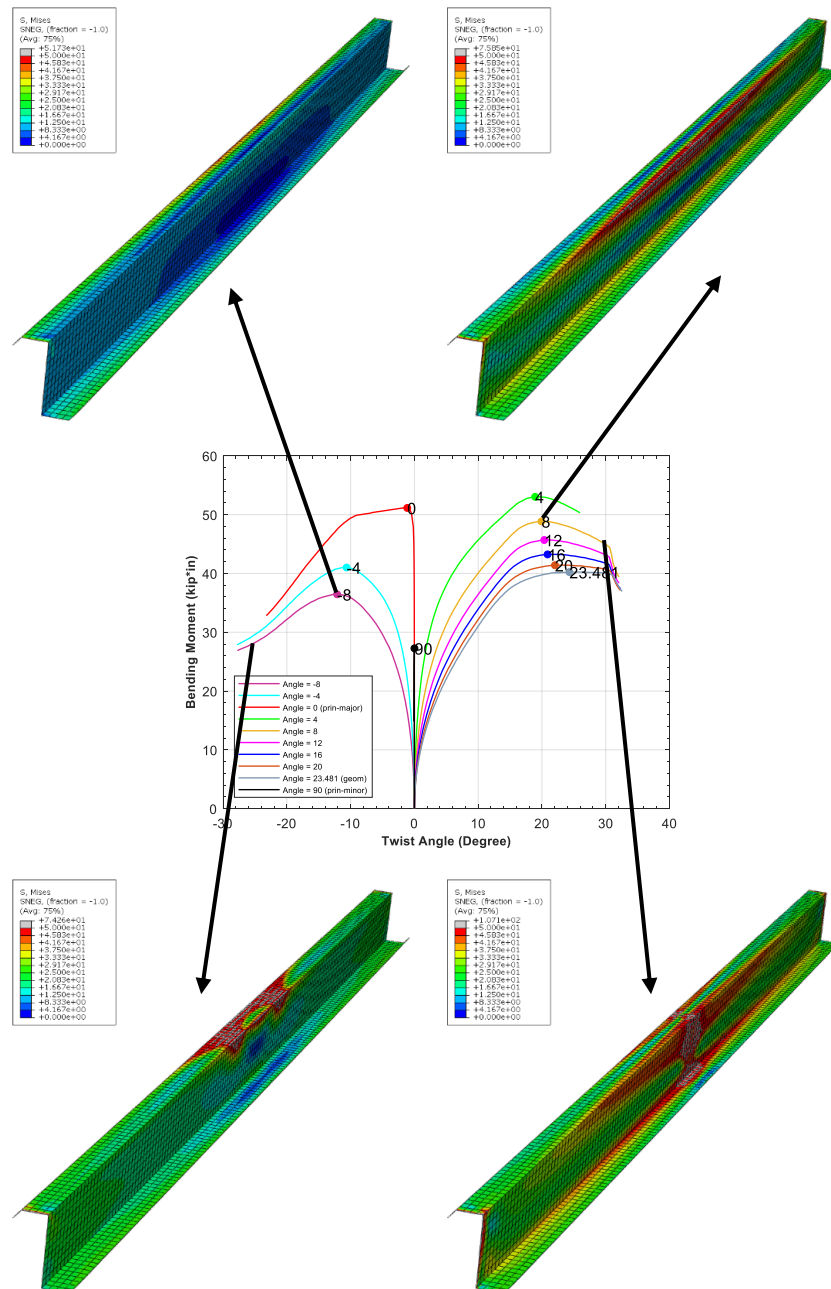

Figure 6: Lateral-torsional buckling in opposite directions for 6ZS2.25×105 with F_y = 50 ksi and L = 144 in.

9

4.2 Failure mode sensitivity to imperfection

Cold-formed steel members have geometric imperfections due to the production process, shipping, and installation. Results are imperfection sensitive when the models have bifurcation; however, the imperfection sensitivity is reduced if primary deformation already exists in the buckling direction, e.g. in these models when twist has already initiated. This section of the paper briefly explores how imperfections impact the LTB flexural capacity for the target sections under bending moment about the major principal axis (a case that should be imperfection sensitive).

For this small study a twist imperfection is applied. Only bending about the major principal axis ($\theta = 0°$) is considered. An L/2292 imperfection is applied to the 6ZS2.25×105 and 10ZS2.25×105 with $F_y = 50$ksi. The imperfection factor was estimated based on a maximum imperfection twist angle of no more than 2 degrees. As shown in Figure 7, introduction of the 2 deg. twist imperfection eliminates the sharp bifurcation nature of the response for the case with bending about the major principal axis ($\theta = 0°$), and provides response in essence equivalent to bending about an axis approximately 2° from the principal axis.
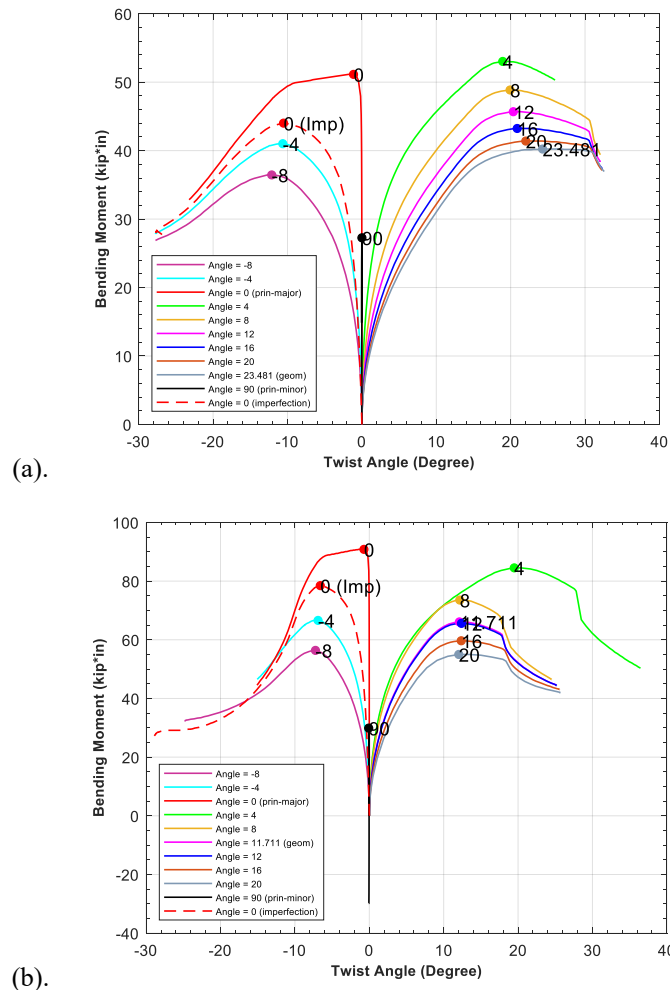

(a).

(b).

Figure 7: Moment-web twist plots for (a) 6ZS2.25×105, (b) 10ZS2.25×105 section with $F_y = 50$ ksi., L = 144 in, and 2 deg. initial twist imperfection.

10

5. Studied Design Methods

Nominal flexural capacity was predicted by three design methods: (1) AISI S100-16 approximate approach, (2) AISI S100-16 linear interaction approach, and (3) a new method considering direct bi-axial bending consistent with recent Direct Strength Method proposals. Note, Trahair (2018) has provided additional design methods for consideration. Here only the first three methods are detailed.

5.1 Method 1: AISI S100-16 Approximate Approach

Method 1 requires critical elastic lateral-torsional buckling stress F_{cre} to be calculated using Eq. F2.1.3-1 from AISI S100-16, which is an approximate expression for point-symmetric sections bending about the geometric axis:

$$F_{cre} = \frac{C_b r_o A}{2S_f} \sqrt{\sigma_{ey}\sigma_t} \tag{5}$$

where C_b is permitted to be conservatively taken as unity for all cases, r_o is the polar radius of gyration of cross-section about shear center, A is the cross-section area, S_f is the elastic section modulus, σ_{ey} and σ_t are the critical axial stress for elastic buckling about y-axis and torsion. The nominal stress F_n is then determined as:

$$\text{for } F_{cre} \geq 2.78F_y, \quad F_n = F_y \tag{6}$$

$$\text{for } 2.78F_y > F_{cre} > 0.56F_y, \quad F_n = \frac{10}{9}F_y\left(1 - \frac{10F_y}{36F_{cre}}\right) \tag{7}$$

$$\text{for } F_{cre} \leq 0.56F_y, \quad F_n = F_{cre} \tag{8}$$

The nominal flexural strength, M_{ne}, is defined by:

$$M_{ne} = S_f F_n \tag{9}$$

Common practice is to consider only bending about the geometric axis. So, if the perpendicular component of the moment is ignored, the strength for the axis of the applied moment is given by Eq. 10 where β is the angle between the axis of bending and the geometric axis.

$$M_n = \frac{M_{ne}}{\cos(\beta)} \tag{10}$$

5.2 Method 2: AISI S100-16 Interaction Approach

Method 2 requires that the strength be calculated independently about the major and minor principal axes, designated as M_{n1} and M_{n2}, then combined in an interaction formula based on the demand. The engineer should calculate the elastic lateral torsional buckling moment, M_{crei}, first yield moment, M_{yi}, and fully plastic moment M_{pi}; where i is either 1 or 2 and refers to bending about the major or minor principal axis to find M_{ni}. M_{crei} can be calculated using Glauz (2017) or CFS or CUFSM. M_{yi} and M_{pi} are calculated from first principles. Calculation of M_{pi} is non-trivial since the plastic neutral axis does not typically coincide with the elastic neutral axis. Full solutions for the studied cases are provided in Wang et al. (2020). M_{pi} need only be considered if inelastic

reserve is allowed in the section. M_{ni} is found similar to method 1, but here we allow the possibility of inelastic reserve. If inelastic reserve is not considered, M_{ni} cannot exceed M_{yi} in Eq. 11 or 12.

$$\text{for } M_{crei} > 18.9M_{yi}, \quad M_{ni} = M_{pi} \tag{11}$$

$$\text{for } M_{crei} > 2.78M_{yi}, \quad M_{ni} = M_{pi} - \left(M_{pi} - M_{yi}\right)\frac{\sqrt{M_{yi}/M_{crei}} - 0.23}{0.37} \tag{12}$$

$$\text{for } 2.78M_{yi} > M_{crei} > 0.56M_{yi}, \quad M_{ni} = \frac{10}{9}M_{yi}\left(1 - \frac{10M_{yi}}{36M_{crei}}\right) \tag{13}$$

$$\text{for } M_{crei} \leq 0.56M_{yi}, \quad M_{ni} = M_{crei} \tag{14}$$

Note, according to AISI S100-16 when local buckling is considered there is a maximum strength that is allowed due to liming the extreme fiber strain to 3 times the yield strain, i.e. $C_{y\ell} = 3$. This implies for all cases the maximum strength must actually be slightly less than M_{pi}, i.e.:

$$M_{ni} \leq M_{yi} + (1 - \frac{1}{C_{y\ell}^2})(M_{pi} - M_{yi}) \tag{15}$$

When these strength expressions are used in the linear interaction equation of AISI S100:

$$\frac{M_1}{M_{n1}} + \frac{M_2}{M_{n2}} \leq 1.0 \tag{16}$$

For the special case of bending by moment M about an arbitrary axis at angle θ, demand $M_1 = M|\cos\theta|$ and $M_2 = M|\sin\theta|$ after substitution and solving for M this provides the moment strength about an arbitrary axis:

$$M_n = \frac{1}{\frac{|\cos\theta|}{M_{n1}} + \frac{|\sin\theta|}{M_{n2}}} \tag{17}$$

5.3 Method 3: Direct Bi-axial Bending Approach
Method 3 considers the axis of bending directly. The strength formulas are familiar, but typically written in terms of global slenderness:

$$\lambda_e = \sqrt{M_y/M_{cre}} \tag{18}$$

$$\text{for } \lambda_e \leq 0.23, \quad M_n = M_p \tag{19}$$

$$\text{for } 0.23 < \lambda_e < 0.60, \quad M_n = M_p - \left(M_p - M_y\right)\frac{\sqrt{M_y/M_{cre}} - 0.23}{0.37} \tag{20}$$

$$\text{for } 0.60 < \lambda_e < 1.34, \quad M_n = \frac{10}{9}\left(1 - \frac{10}{36}\lambda_e^2\right)M_y \tag{21}$$

$$\text{for } 1.34 < \lambda_e, \quad M_n = M_{cre} \tag{22}$$

Note, as in Method 2 Eq. 15, due to local buckling limitations:

$$M_n \leq M_y + (1 - \frac{1}{9})(M_p - M_y) \tag{23}$$

In the preceding, M_y, M_p, and M_{cre} are for bending about the arbitrary axis. M_y is readily defined by first yield at an extreme fiber, M_p is more complex for bending about an arbitrary axis and calculations are detailed in Wang et al. (2020), M_{cre} may be determined using CUFSM or CFS elastic LTB analysis, or as an alternative method, M_{cre} can be determined using the analytical method developed in Glauz (2017).

6. Evaluation of Design Methods

The simulation-to-predicted strength ratios for the three design methods are summarized in Table 4 (results for every simulation are provided in Wang et al. 2020). Results are categorized by section and inclination angle for the axis of bending and broken out by relative slenderness, λ_e, with Low less than 0.6, Medium between 0.6 and 1.5, and High greater than 1.5. In addition, the overall accuracy of the studied design methods is assessed in Figure 8. The results show Method 3 to be the most accurate, and that for the stocky/low slenderness cases Methods 2 and 3 essentially converge. Although Method 1 appears reasonable in Figure 8, as Table 4 makes clear Method 1 can be largely unconservative or conservative and limitations on the applicability of Method 1 are needed.

Table 4: Simulation-to-predicted ratios summary for all three methods
(Excluding 6ZS2.25×105 with L = 240 inches).

| Section & θ	Ave. of $M_{max1}/M_{n,1}$			Ave. of $M_{max1}/M_{n,2}$			Ave. of $M_{max1}/M_{n,3}$			Ave. of $M_{max1}/M_{n,1}$	Ave. of $M_{max1}/M_{n,2}$	Ave. of $M_{max1}/M_{n,3}$
	Low	Medium	High	Low	Medium	High	Low	Medium	High			
10ZS2.25×105	**0.13**	**1.05**	**1.54**	**0.99**	**1.11**	**1.26**	**0.99**	**0.85**	**1.09**	**1.10**	**1.14**	**0.93**
-8		0.86	1.16		0.89	0.99		0.77	0.86	0.92	0.91	0.79
-4		1.00	1.18		0.90	0.95		0.79	0.86	1.07	0.92	0.82
0		1.38	1.39		1.00	1.00		1.00	1.00	1.39	1.00	1.00
4		1.30	1.66		1.14	1.30		0.95	1.18	1.44	1.20	1.04
8		1.14	1.59		1.17	1.33		0.88	1.11	1.32	1.23	0.97
11.711		1.08	1.84		1.18	1.55		0.85	1.27	1.23	1.26	0.94
12		1.07	1.83		1.19	1.56		0.85	1.27	1.22	1.26	0.94
16		0.98	1.84		1.21	1.64		0.83	1.25	1.15	1.29	0.92
20		0.91	1.86		1.23	1.74		0.82	1.25	1.10	1.33	0.91
90	0.13			0.99			0.99			0.13	0.99	0.99
6ZS2.25×105	**0.31**	**1.09**	**1.28**	**1.00**	**1.21**	**1.18**	**1.00**	**1.00**	**1.08**	**1.05**	**1.19**	**1.01**
-8		0.82			0.94			0.83		0.82	0.94	0.83
-4		0.92	1.00		0.94	0.97		0.86	0.90	0.94	0.95	0.87
0		1.19	1.19		1.04	1.03		1.04	1.03	1.19	1.04	1.04
4		1.26	1.36		1.23	1.25		1.08	1.15	1.31	1.24	1.11
8		1.19	1.42		1.24	1.35		1.02	1.16	1.25	1.27	1.06
12		1.13	1.42		1.27	1.40		1.01	1.13	1.21	1.30	1.04
16		1.17			1.34			1.04		1.17	1.34	1.04
20		1.15			1.38			1.05		1.15	1.38	1.05
23.481		1.13			1.41			1.07		1.13	1.41	1.07
90	0.31			1.00			1.00			0.31	1.00	1.00
Grand Total (Mean)	**0.21**	**1.07**	**1.45**	**0.99**	**1.16**	**1.23**	**0.99**	**0.92**	**1.09**	**1.08**	**1.16**	**0.97**
Grand Total (COV)	**0.52**	**0.16**	**0.19**	**0.15**	**0.15**	**0.21**	**0.15**	**0.14**	**0.14**	**0.36**	**0.18**	**0.16**
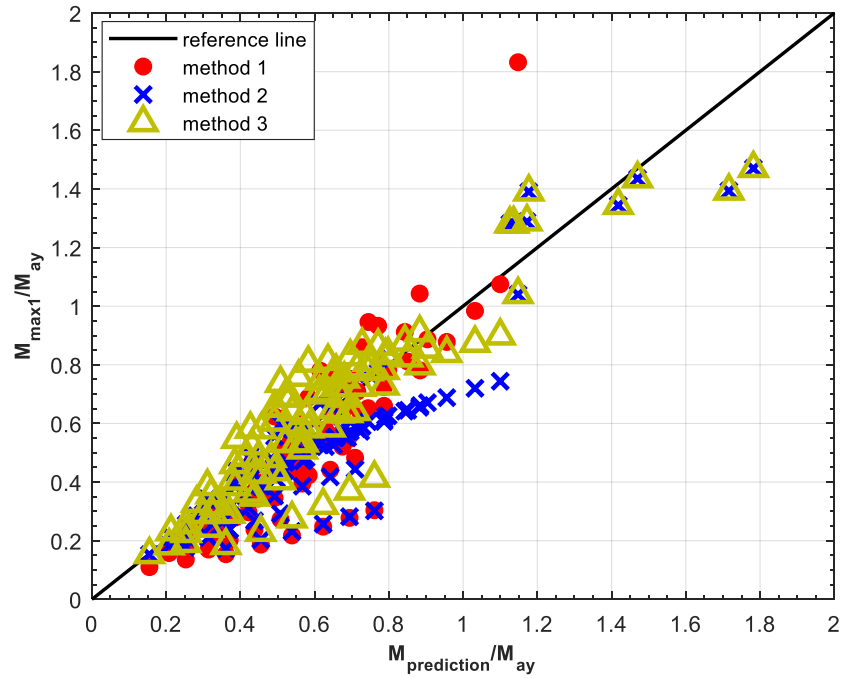
Figure 8: Simulation versus prediction for the three methods about all cases (With Range limitation).

Method 2 uses an interaction equation approach to strength prediction, therefore directly examining the performance against the interaction equation in AISI provides a useful assessment of the method as shown in Figure 9. Method 2 is consistently conservative.
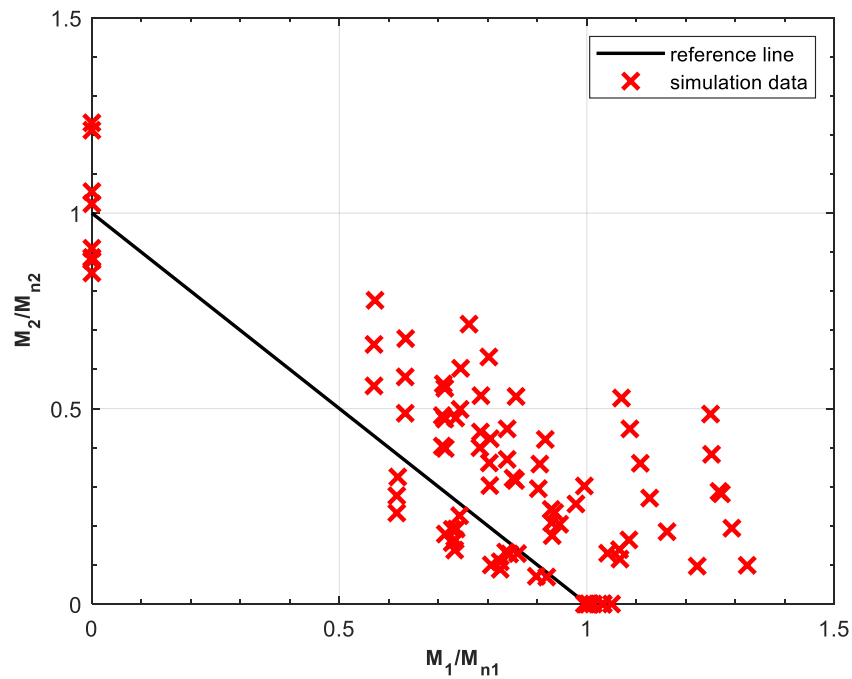

Figure 9: linear interaction for all cases (with inelastic reserve, exclude 6ZS2.25×105 with L = 240 inches).

Given that Method 2 is most naturally assessed through examination of the interaction expressions it may be insightful to view Method 3's predicted interaction expression – i.e. what does the prediction of Method 2 look like when plotted in the biaxial bending interaction space. An example of such a plot is are provided in Figure 10, where M_{n1} and M_{n2} are the principal axis components of M_n determined using Method 3. These curves indicate the significant improvement that Method 3 is able to make on the classic interaction expression – and provide further support for its recommendation as a primary method of strength prediction.
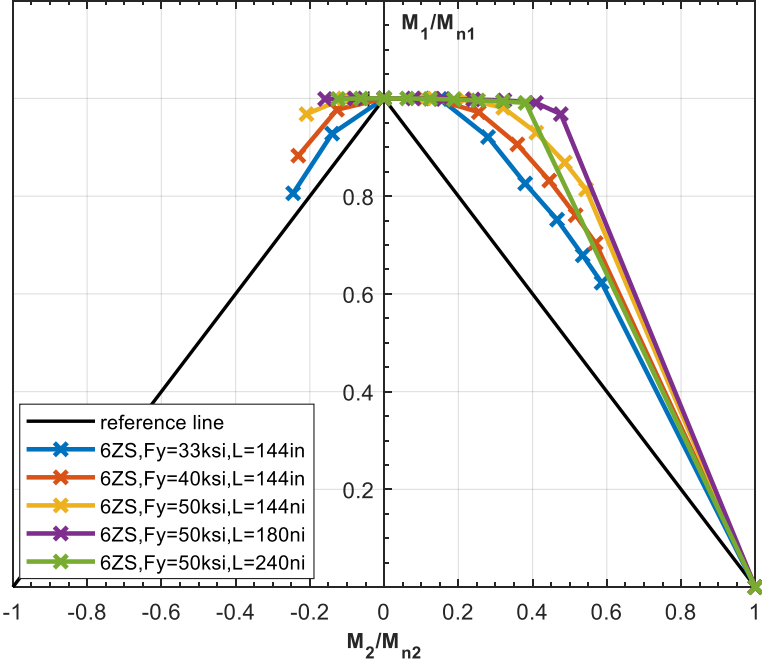

Figure 10: Method 3 compares with linear reference line for 6ZS2.25×105.

Method 3 is essentially a variant of the Direct Strength Method. As such, the method can be compared in a classical slenderness vs. strength plot as provided in Figure 11. In all of the data reported in this section the L=240 in. 6ZS2.25x105 results have been removed. This section rotates and plastifies about its minor axis and does not exhibit buckling in any meaningful sense.
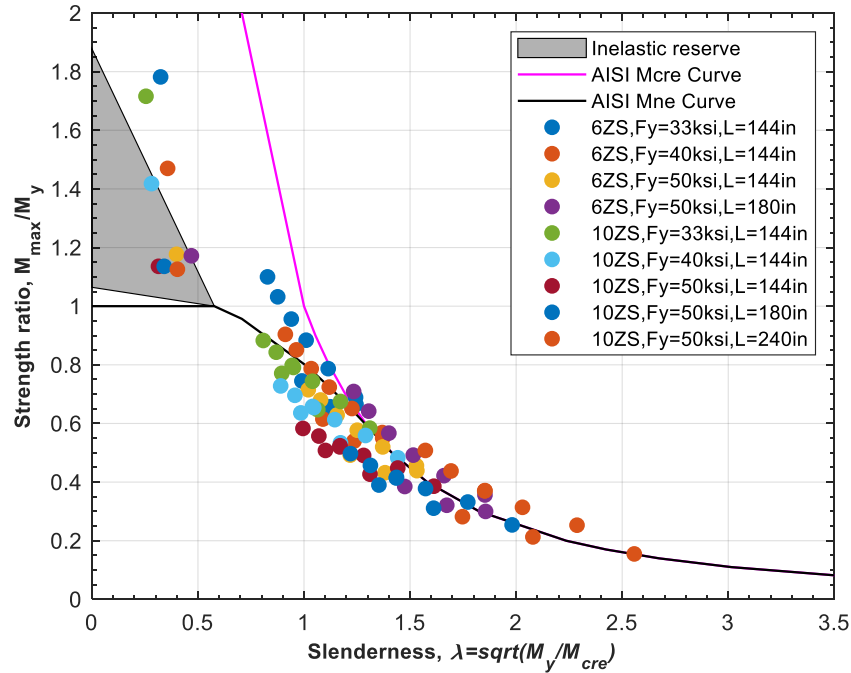
Figure 11: Strength ratio versus slenderness for all cases from ABAQUS collapse analysis (With case detail, excluding 6ZS2.25×105 with L = 240 inches).

7. Conclusions

Applications for non-symmetric cold-formed steel members commonly induce biaxial bending since loads are almost never aligned with the principal axes of the section. Recently, Glauz (2017) developed an analytical solution for the lateral-torsional buckling (LTB) moment (M_{cre}) of a non-symmetric section bent about an arbitrary axis. These provisions could potentially replace simplified expressions used in AISI-S100-16 for M_{cre}; however, the impact of applying this expression in design has not been fully assessed for LTB limit states. To assess the implications of employing the more accurate M_{cre} solution, a series of shell finite element collapse analyses were performed on two Zee-sections: 6ZS2.25×105 and 10ZS2.25×105, previously identified to be controlled by LTB, as opposed to local or distortional buckling. The collapse simulations were performed on sharp corner models of the Zee shapes under isolated and equal end moments and were augmented by eigenvalue buckling analysis in ABAQUS and finite strip method analyses conducted in CUFSM and in CFS. All of the ABAQUS shell finite element collapse simulations converged at large enough deformations to achieve at least one peak moment.

Three design approaches were compared to the conducted simulations: (1) AISI-S100-16 approximate approach, (2) AISI-S100-16 interaction approach, and (3) direct bi-axial bending approach. For method 1, the AISI S100-16 approximate approach uses a conservatively low estimate of M_{cre}, but ignores bending about anything other than the geometric axis – this combination of conservative and unconservative assumptions balances out as long as the bending axis is reasonably close to the geometric axis – for large deviations it is problematic and invalid. For method 2, the AISI-S100-16 interaction approach uses the elastic buckling and strength about the major- and minor-principal axes as anchors and gives reasonable predictions, but can be overly conservative particularly if inelastic reserve is ignored. For method 3, the direct bi-axial bending

16

approach is a rational extension of the Direct Strength Method and uses the buckling and yielding solutions about the arbitrary axis of bending – and is shown to provide the best overall prediction of the strength. Many of the bi-axial bending finite element collapse simulations exhibited large rotations which would likely be deemed unacceptable in practice. Future study would be appropriate to estimate the rotation and establish serviceability limits or guidelines. In addition, this study did not assess the impact of moment gradient, nor that of local or distortional buckling for bending about arbitrary axes.

Acknowledgments

References

ABAQUS (version 6.13), Simulia, Inc.

AISI D100 (2017), Cold-Formed Steel Design Manual, American Iron and Steel Institute, Washington, DC, Vol. 1.

AISI S100 (2016), North American Specification for the Design of Cold-Formed Steel Structural Members. American Iron and Steel Institute, Washington, DC.

CFS [Cold-Formed Steel Design Software] (Version 12). RSG Software, Inc., Retrieved from https://www.rsgsoftware.com

CUFSM [Cold-Formed Steel Design Software] (version 5.03). Thin-walled structures lab at Johns Hopkins University, Retrieved from https://www.ce.jhu.edu/bschafer/cufsm/

Glauz, R.S. (2017). "Elastic lateral-torsional buckling of general cold-formed steel under uniform moment." *Thin-Walled Structures*, 119 (2017) 586-592.

Trahair, N.S. (2018). "Non-linear biaxial bending of steel Z-beam." *Thin-Walled Structures*, 129 (2018) 317-326.

Wang, S., Glauz, R.S., Schafer, B.W. (2020). "Inelastic lateral-torsional buckling strength validation for non-principal axis bending using numerical methods." *Cold-Formed Steel Research Consortium*, R-2020-01. Access at http://jhir.library.jhu.edu/handle/1774.2/62110

Zeinoddini, V., Schafer, B.W. (2011). "Global Imperfections and dimensional variations in cold-formed steel members." *International Journal of Structural Stability and Dynamics*, Vol.11, No.5 (2011) 827-854.